Metal-Ligand Complexation through Redox Assembly at Surfaces Characterized by Vibrational Spectroscopy

Christopher G. Williams,[1] Miao Wang,[2] Daniel Skomski,[1] Christopher D. Tempas,[1]

Larry L. Kesmodel,[2] and Steven L. Tait[1,2,*]

[1] Dept. of Chemistry, Indiana University

[2] Dept. of Physics, Indiana University

* E-mail: tait@indiana.edu, Tel: +1-812-855-1302

Supplemental Materials

Normalization of HREEL Spectra

Full range scans (150-3500 cm^{-1}) were normalized by the average intensity of the flat background region from 3693-3723 cm^{-1}. The higher resolution scans for out-of-plane and in-plane ring modes (550-2000 cm^{-1}) were normalized to the 1920-1950 cm^{-1} region. The higher resolution C-H stretching mode spectra (2600-3600 cm^{-1}) were normalized to the 2630-2659 cm^{-1} region, then a linear background was subtracted from the spectra for clarity in interpreting the peak. Low energy scans (-50-600 cm^{-1}) did not have a sufficient featureless spectral region for normalization so these were normalized to the elastic scattering peak.

Scanning Tunneling Microscopy Measurements of DPTZ and of DPTZ+Pt on Ag(111)

Scanning tunneling microscopy measurements were made for DPTZ on Ag(111). A high degree of ordering of the DPTZ molecules is observed in two different packing structures (Figure S1). Note that corresponding measurements for Pt-DPTZ on Au(100) have been reported previously.[1]

Figure S2 shows an image after Pt-DTPZ on Ag(111) is annealed at 200 °C, then cooled to room temperature for imaging. As discussed in the manuscript, HREELS indicates that this leads to complexation to Ag, which shows a relatively disordered structure. XPS indicates a reduction of Pt during this exchange. It is expected that this Pt will form into nanoparticles on the surface, such as the large bright nanoparticle feature in Figure S2.

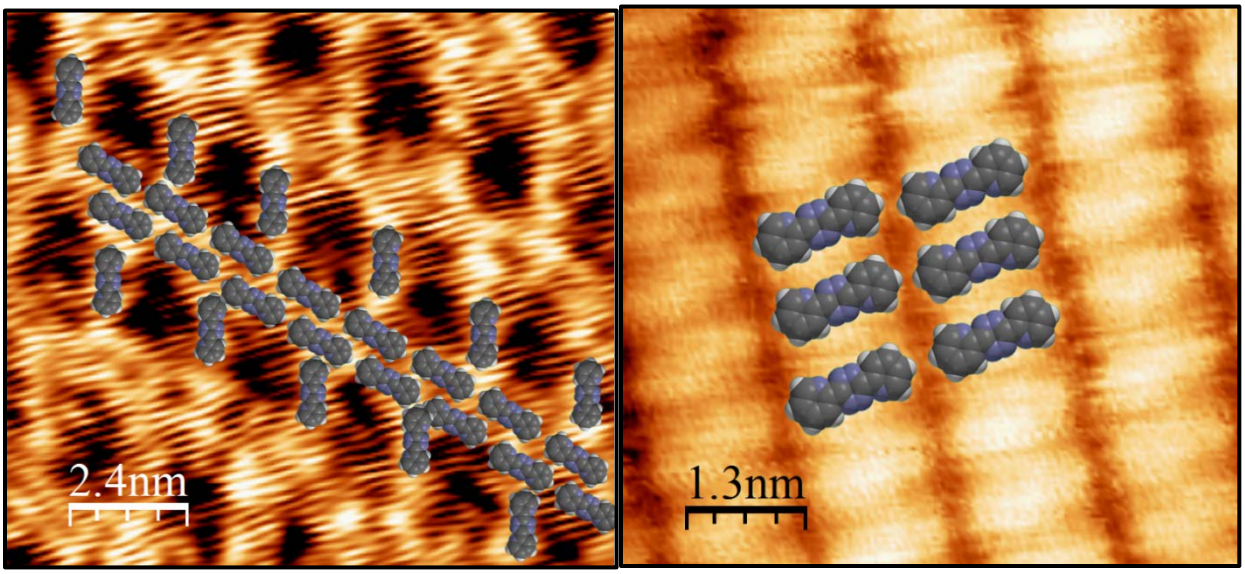

Figure S1. STM images of DPTZ on Ag(111). Two packing structures were observed, as shown here, but note that the lower density structure on the left is relatively rare. (STM parameters: 1.3 V tip-surface bias and 10 pA set-point tunneling current for both images.)

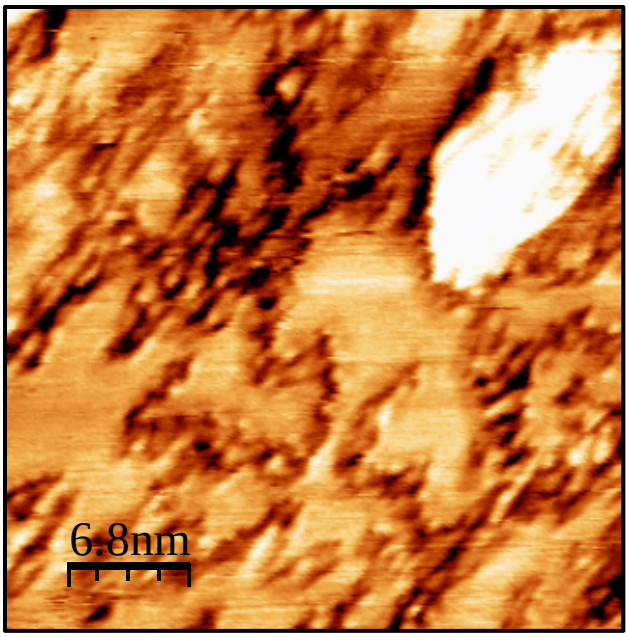

Figure S2. DPTZ annealed with Pt present at 200 °C for 55 minutes on Ag(111). No ordered 1D chains are observed. Instead a more disordered chain growth is observed. The large bright feature may be a Pt nanoparticle. (STM parameters: 1.3 V tip-surface bias and 8.4 pA set-point tunneling current.)

Supplemental HREELS Data

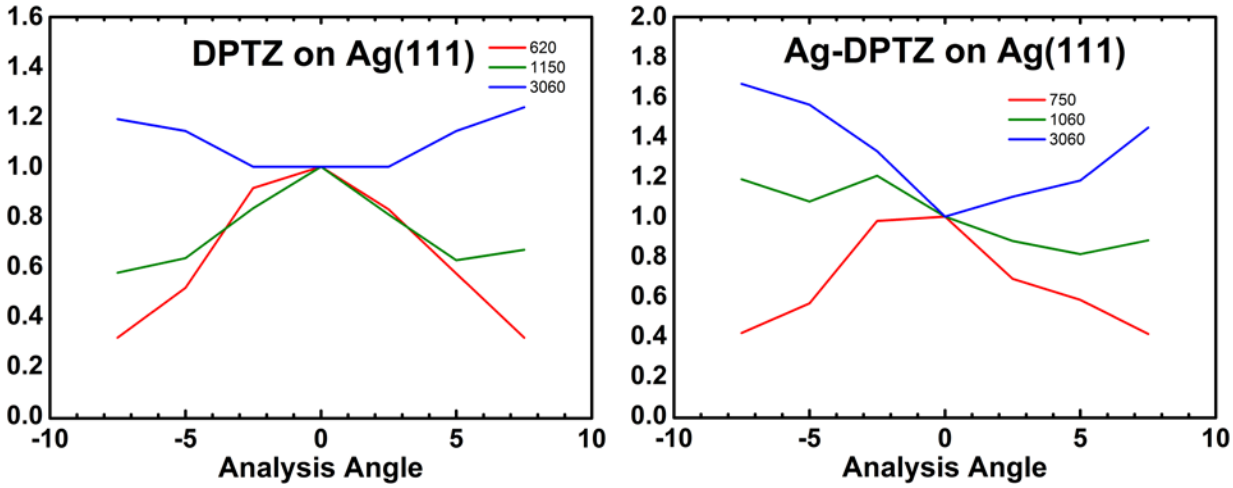

Figure S3. Off-specular analysis of specific HREELS peak intensities for (left) DPTZ and (right) Ag+DPTZ annealed above 170 °C on Ag(111). The spectral analysis angle is 0°. 620 and 750 cm^{-1} are out-of-plane modes for the pyridine rings of the molecule and complex, 1150 and 1060 cm^{-1} are in-plane modes of the molecule, and 3060 cm^{-1} is the C-H stretch. HREELS is sensitive to dipole scattering and impact scattering of the electron beam, but only the former has a strong selection rule for changing dipole moments perpendicular to the surface. The dipole scattering intensity drops sharply as the detector moves away from the specular, thus an off-specular drop in intensity indicates a predominantly dipole scattering mode. The feature with the greatest off-specular change in these experiments is the pyridine out-of-plane mode (decreases to 40% of original height), indicating that this out-of-plane mode is perpendicular to the surface for DPTZ and Ag-DPTZ. Thus, the orientation of the molecule before and after coordination is flat on the surface. The small changes to the in-plane mode and C-H stretching modes support this orientation.

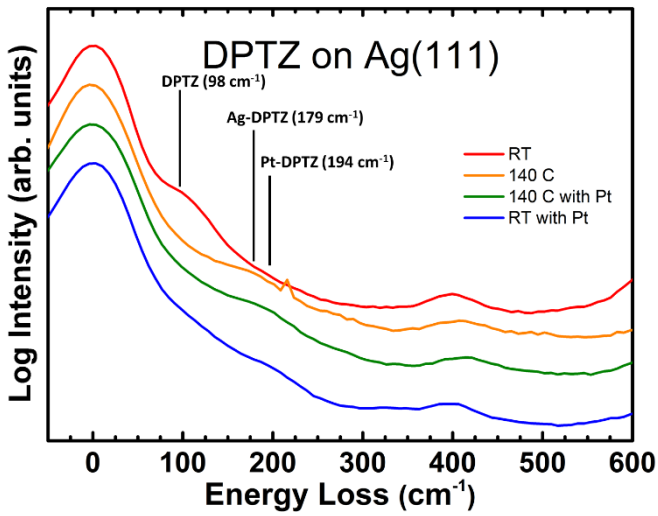

Figure S4. Low energy peaks for DPTZ without coordination at room temperature (RT), when coordinated to Ag (140 °C anneal with and without Pt), and coordinated to Pt (RT with Pt). We can see the appearance of a new peak at 179 cm^{-1} for Ag coordination, but 194 cm^{-1} for Pt coordination. This is in agreement with previous metal dependent stretches that has the Ag-N coordination at a lower energy than Pt-N.[2]

Electron-stimulated Desorption of DPTZ

DPTZ was found to be susceptible to electron-stimulated desorption (ESD) from either surface with both LEED and AES. The molecule desorbed under a 1.5 keV AES electron beam in less than 5 minutes from either surface and subsequent HREELS did not detect any DPTZ on the surface. Self-metallated Ag-DPTZ on Ag(111) and Pt-DPTZ on Au(100) were also seen to desorb under the AES beam. In the case of Pt-DPTZ on Ag(111), a steady AES C peak was observed for up to one hour, but HREELS revealed that there had been significant chemical changes in the adsorbate layer.

As for LEED, an adlayer pattern for the organic species could be observed around 50 eV (Figure S9) for 0.75 ML of material on Ag(111) but only for a couple minutes before the pattern disappeared. This pattern could be regenerated by moving to another location, but only a couple minutes at the new location could be utilized before the pattern disappeared. This is in agreement with STM observations that some ordering of the DPTZ molecules could be seen on the Ag(111) surface (Figure S1). No LEED pattern of submonolayer DPTZ on Au(100) was observed, and no LEED pattern could be observed after the DPTZ had undergone complexation with a metal on Ag(111) or Au(100). Even though chains are visible via STM on Au(100) it appears they are not crystalline enough to produce a LEED pattern or they are too susceptible to ESD.

Low-energy Electron Diffraction of DPTZ on Ag(111)

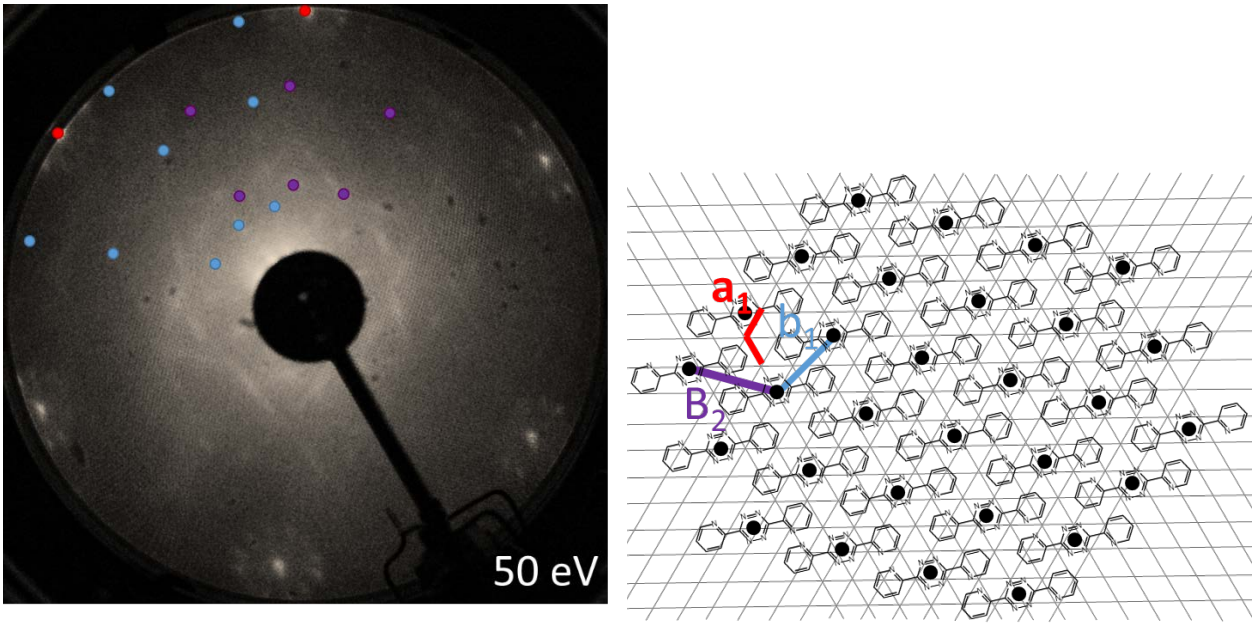

Figure S5. LEED of 0.75 ML DPTZ on Ag(111) at room temperature. The pattern degrades in a few minutes under the LEED beam. LEED patterns of DPTZ on Au(100) could not be obtained, presumably due to electron-stimulated desorption. There are a set of 12 spots in the pattern at 2.5 (purple) and at 1.5 times (blue) less than the Ag lattice atom spot spacing (red). The blue is too small of a spacing to correspond to a molecular distance, so this is likely the second spot in that diffraction direction. The first spot is thus likely 2.9 times less than the Ag atom spot spacing. This corresponds to distances of 0.732 nm with the other unit cell vector being 0.838 nm with the Ag nearest neighbor distance of 0.289 nm. The formation of three different domains on the surface generates the ring of 12 spots observed at each of these distances. The angle between these two distances is about 120° with the smaller being 18° rotated off the lattice.

Standard Electrode Potentials for Relevant Metal Reduction/Oxidation Steps

Here, we compile standard electrode potentials from the reference literature for reactions relevant to the redox processes discussed in the paper.[3-4] These are given as standard electrode potentials in aqueous solutions at 25 °C and 1 atm as V vs. NHE. We used these to calculate potential Pt replacement reactions with Ag or Au. Interestingly, the Ag/Ag^{+} and Pt^{2+}/Pt exchange is spontaneous, while Pt^{2+} replacement by Au is not. Although there are certainly many other factors affecting the surface chemistry reported in the manuscript. It is interesting to note that these values are consistent with our experimental observation of Pt replacement by Ag adatoms, but not by Au.

		V vs. NHE
$Pt^{2+} + 2e^- \rightleftharpoons Pt$		1.188
$Ag^{+} + e^- \rightleftharpoons Ag$		0.7991
$Ag^{2+} + e^- \rightleftharpoons Ag^{+}$		1.980
$Au^{+} + e^- \rightleftharpoons Au$		1.83
$Au^{2+} + e^- \rightleftharpoons Au^{+}$		1.8
$Au^{3+} + 3e^- \rightleftharpoons Au$		1.52

$$PtDPTZ + 2Ag^0 \rightleftharpoons Ag_2DPTZ + Pt^0$$

$$Pt^{2+} + 2Ag^0 \rightleftharpoons 2Ag^{+} + Pt^0 \qquad E_{cell} = 0.3889\ V$$

$$3PtDPTZ + 2Au^0 \rightleftharpoons Au_2DPTZ_3 + 3Pt^0$$

$$3Pt^{2+} + 2Au^0 \rightleftharpoons 2Au^{3+} + 3Pt^0 \qquad E_{cell} = -0.332\ V$$

$$PtDPTZ + 2Au^0 \rightleftharpoons Au_2DPTZ + Pt^0$$

$$Pt^{2+} + 2Au^0 \rightleftharpoons 2Au^{+} + Pt^0 \qquad E_{cell} = -0.642\ V$$

DFT Calculations of Vibrational Modes

DFT calculations were made using the Gaussian 09 software package.[5] The B3LYP 6-31G* basis set was used for DPTZ while a mix basis set of B3LYP 6-31G* and LanL2DZ was used for Pt-DPTZ, consistent with prior computational work.[6-7] These calculations were used to help in the interpretation and assignment of HREELS data, particularly out-of-plane vs in-plane vibrational modes. The DFT also helped in identification of the primary C-H bending mode between 700-800 cm^{-1} and aided in the groupings of in-plane modes. Atomic coordinate data is given for DPTZ in Table S1 and for Pt-$DPTZ_2$ in Table S2. Vibrational mode results from the DFT calculations for DPTZ are listed in Table S3 and those for Pt-$DPTZ_2$ are listed in Table S4.

Vibrational modes below 1000 cm^{-1} were scaled by a factor of 0.9842 while those above 1000 cm^{-1} were scaled by 0.9674, in accordance with previous literature using the Gaussian 09 software.[8] Due to the symmetry of the molecules and the presence of the inversion center, all the gerade vibrational modes have zero intensity. The surface would break this inversion center symmetry and so they could exhibit non-zero intensity in the HREELS experiment.

The intensities in Table S3 and S4 are scaled relative to the most intense feature above 250 cm^{-1} as lower energy features are usually obscured by the elastic scattering peak in HREELS experiments.

In Tables S3 and S4, we report the intensities of the vibrational modes in four different ways. The magnitude squared of the derivative of the molecular dipole with respect to the vibrational motion, $\left|\frac{\delta P}{\delta Q_\alpha}\right|^2$, is the typical intensity output for each vibrational mode from Gaussian (fourth column of Tables S3 and S4). This intensity is most closely associated with

typical IR techniques where the molecules are not oriented in a specific manner and integrated IR intensity of a mode α is given by:

$$A_\alpha = \frac{N\pi}{3c^2}\left|\frac{\delta P}{\delta Q_\alpha}\right|^2 .$$

This is useful in estimating HREELS impact scatting mode intensities, which do not depend on dipole selection rules. Their intensities at increasing frequencies are known to decrease by a factor inversely proportional to the frequency,[9] so these intensities can be estimated as $\frac{1}{f_\alpha}\left|\frac{\delta P}{\delta Q_\alpha}\right|^2$ (fifth column of Tables S3 and S4).

Due to surface selection rules, the HREELS dipole scattering mode intensity will be proportional to the derivative of the dipole *z*-component:

$$A'_\alpha = \frac{N\pi}{3c^2}\left|\frac{\delta P_z}{\delta Q_\alpha}\right|^2 .$$

With the assumption that the molecules are flat-lying on the surface, we can define the *z*-direction in the calculation as the direction perpendicular to the molecular plane to estimate the dipole scattering intensity. The quantity $\left|\frac{\delta P_z}{\delta Q_\alpha}\right|^2$ is presented in the sixth column of Tables S3 and S4. The intensities of dipole scattering modes decrease with increasing frequency by a factor of $1/f^3$, so we estimate their intensities as $\frac{1}{f_\alpha^3}\left|\frac{\delta P_z}{\delta Q_\alpha}\right|^2$ in the seventh column of Tables S3 and S4.[9] Each HREELS vibrational mode is some combination of dipole and impact scattering intensities.

Table S1. Atomic coordinate data for DPTZ resulting from DFT calculations.

Atom Number	Atomic Number	X	Y	Z
1	7	1.185707	-0.65034	0
2	7	1.195206	0.664465	0
3	6	0.000929	1.289639	0
4	7	-1.18571	0.65034	0
5	7	-1.19521	-0.66447	0
6	6	-0.00093	-1.28964	0
7	6	0.031825	-2.7762	0
8	1	2.186144	-2.88388	0
9	6	1.262377	-3.44987	0
10	1	2.190601	-5.39468	0
11	6	1.255188	-4.84211	0
12	1	-0.02096	-6.59412	0
13	6	0.031825	-5.50948	0
14	1	-2.1135	-5.22896	0
15	6	-1.13839	-4.74454	0
16	7	-1.15111	-3.41124	0
17	6	-0.03183	2.776202	0
18	1	-2.18614	2.883884	0
19	6	-1.26238	3.449865	0
20	1	-2.1906	5.394677	0
21	6	-1.25519	4.842113	0
22	1	0.020956	6.594115	0
23	6	-0.03183	5.509484	0
24	1	2.113495	5.228962	0
25	6	1.138385	4.744538	0
26	7	1.151108	3.411237	0

Table S2. Atomic coordinate data for Pt-DPTZ$_2$ resulting from DFT calculations.

Atom Number	Atomic Number	X	Y	Z
1	78	0	0	0
2	6	-2.2485	2.103475	0
3	1	-1.41864	2.802899	0
4	6	-3.56837	2.523433	0
5	1	-3.77478	3.588138	0
6	6	-4.60448	1.575677	0
7	1	-5.64423	1.888671	0
8	6	-4.27586	0.231557	0
9	1	-5.0206	-0.55601	0
10	7	-3.32573	-2.51444	0
11	7	-2.87015	-3.76209	0
12	6	-1.50466	-3.90335	0
13	7	-0.62067	-2.92819	0
14	6	-0.98791	-5.29915	0
15	6	-1.88951	-6.37342	0
16	1	-2.95355	-6.17186	0
17	6	-1.38128	-7.67073	0
18	1	-2.0552	-8.52313	0
19	6	0	-7.85357	0
20	1	0.441683	-8.84557	0
21	6	0.814306	-6.71689	0
22	1	1.898613	-6.82027	0
23	7	0.346976	-5.46786	0
24	6	2.248503	-2.10348	0
25	1	1.418635	-2.8029	0
26	6	3.568365	-2.52343	0
27	1	3.774777	-3.58814	0
28	6	4.604475	-1.57568	0
29	1	5.64423	-1.88867	0
30	6	4.275861	-0.23156	0
31	1	5.020604	0.556006	0
32	7	3.325731	2.514444	0
33	7	2.870148	3.762086	0
34	6	1.504656	3.90335	0
35	7	0.620669	2.928185	0
36	6	0.987914	5.299152	0
37	6	1.88951	6.373424	0
38	1	2.953551	6.171858	0
39	6	1.381278	7.670732	0

40	1	2.055204	8.523131	0
41	6	0	7.853568	0
42	1	-0.44168	8.845571	0
43	6	-0.81431	6.716889	0
44	1	-1.89861	6.820267	0
45	7	-0.34698	5.467856	0
46	6	-2.47348	-1.50671	0
47	6	-2.92611	-0.14215	0
48	6	2.926109	0.142149	0
49	6	2.473483	1.506707	0
50	7	1.919724	-0.78863	0
51	7	1.092397	1.661945	0
52	7	-1.91972	0.788627	0
53	7	-1.0924	-1.66195	0

Table S3. Vibrational modes and relative intensities from DFT calculations for DPTZ. The columns present: (1) mode number, (2) symmetry element, (3) frequency, and (4-7) four estimates of intensity, as discussed in the text. Each of the intensity columns are normalized to the most intense feature above 250 cm^{-1}. Peaks in HREEL spectra include intensity from both impact scattering and dipole scattering modes, which are best estimated by $\frac{1}{f_\alpha}\left|\frac{\delta P}{\delta Q_\alpha}\right|^2$ (column 5) and by $\frac{1}{f_\alpha^3}\left|\frac{\delta P_z}{\delta Q_\alpha}\right|^2$ (column 7), respectively.[9]

Mode, α	sym	frequency, f_α (cm^{-1})	$\left\|\frac{\delta P}{\delta Q_\alpha}\right\|^2$	$\frac{1}{f_\alpha}\left\|\frac{\delta P}{\delta Q_\alpha}\right\|^2$	$\left\|\frac{\delta P_z}{\delta Q_\alpha}\right\|^2$	$\frac{1}{f_\alpha^3}\left\|\frac{\delta P_z}{\delta Q_\alpha}\right\|^2$
1	AU	5	0.0006	0.1635	0.0031	4924.0194
2	AU	26	0.0212	1.1327	0.1068	1382.7041
3	BG	38	0.0000	0.0000	0.0000	0.0000
4	BU	83	0.0150	0.2551	0.0000	0.0000
5	BG	114	0.0000	0.0000	0.0000	0.0000
6	AU	156	0.0012	0.0108	0.0061	0.3717
7	AG	186	0.0000	0.0000	0.0000	0.0000
8	AG	232	0.0000	0.0000	0.0000	0.0000
9	AU	318	0.0004	0.0016	0.0018	0.0134
10	BG	323	0.0000	0.0000	0.0000	0.0000
11	BU	397	0.0037	0.0130	0.0000	0.0000
12	AU	402	0.0016	0.0055	0.0080	0.0287
13	BG	408	0.0000	0.0000	0.0000	0.0000
14	BU	423	0.0141	0.0470	0.0000	0.0000
15	AU	426	0.0450	0.1482	0.2270	0.6860
16	AG	493	0.0000	0.0000	0.0000	0.0000
17	BG	538	0.0000	0.0000	0.0000	0.0000
18	AU	616	0.1981	0.4517	1.0000	1.0000
19	AG	617	0.0000	0.0000	0.0000	0.0000
20	BU	622	0.0254	0.0574	0.0000	0.0000
21	AG	664	0.0000	0.0000	0.0000	0.0000
22	AG	683	0.0000	0.0000	0.0000	0.0000
23	BU	738	0.0667	0.1268	0.0000	0.0000
24	BG	750	0.0000	0.0000	0.0000	0.0000
25	AU	750	0.0988	0.1848	0.4987	0.2754
26	BG	783	0.0000	0.0000	0.0000	0.0000
27	AU	809	0.0895	0.1552	0.4516	0.1989
28	AG	834	0.0000	0.0000	0.0000	0.0000
29	BG	858	0.0000	0.0000	0.0000	0.0000
30	AU	917	0.0054	0.0083	0.0274	0.0083
31	BG	918	0.0000	0.0000	0.0000	0.0000
32	AU	973	0.0019	0.0027	0.0094	0.0024
33	BG	973	0.0000	0.0000	0.0000	0.0000
34	AG	979	0.0000	0.0000	0.0000	0.0000

35	BU	979	0.0437	0.0615	0.0000	0.0000
36	AU	988	0.0006	0.0008	0.0031	0.0007
37	BG	988	0.0000	0.0000	0.0000	0.0000
38	BU	994	0.0836	0.1161	0.0000	0.0000
39	AG	1027	0.0000	0.0000	0.0000	0.0000
40	BU	1035	0.0169	0.0225	0.0000	0.0000
41	BU	1045	0.0577	0.0762	0.0000	0.0000
42	AG	1059	0.0000	0.0000	0.0000	0.0000
43	BU	1089	0.0186	0.0236	0.0000	0.0000
44	AG	1091	0.0000	0.0000	0.0000	0.0000
45	BU	1125	0.3190	0.3911	0.0000	0.0000
46	BU	1148	0.0035	0.0042	0.0000	0.0000
47	AG	1148	0.0000	0.0000	0.0000	0.0000
48	BU	1248	0.0137	0.0151	0.0000	0.0000
49	AG	1271	0.0000	0.0000	0.0000	0.0000
50	BU	1283	0.2078	0.2235	0.0000	0.0000
51	AG	1283	0.0000	0.0000	0.0000	0.0000
52	AG	1314	0.0000	0.0000	0.0000	0.0000
53	BU	1330	0.0199	0.0207	0.0000	0.0000
54	BU	1380	1.0000	1.0000	0.0000	0.0000
55	AG	1421	0.0000	0.0000	0.0000	0.0000
56	BU	1438	0.0502	0.0482	0.0000	0.0000
57	AG	1453	0.0000	0.0000	0.0000	0.0000
58	AG	1462	0.0000	0.0000	0.0000	0.0000
59	BU	1475	0.0102	0.0095	0.0000	0.0000
60	AG	1486	0.0000	0.0000	0.0000	0.0000
61	BU	1579	0.1224	0.1069	0.0000	0.0000
62	AG	1580	0.0000	0.0000	0.0000	0.0000
63	AG	1588	0.0000	0.0000	0.0000	0.0000
64	BU	1588	0.0734	0.0637	0.0000	0.0000
65	BU	3074	0.1806	0.0810	0.0000	0.0000
66	AG	3074	0.0000	0.0000	0.0000	0.0000
67	BU	3097	0.0730	0.0325	0.0000	0.0000
68	AG	3097	0.0000	0.0000	0.0000	0.0000
69	BU	3114	0.1773	0.0785	0.0000	0.0000
70	AG	3114	0.0000	0.0000	0.0000	0.0000
71	AG	3141	0.0000	0.0000	0.0000	0.0000
72	BU	3141	0.0083	0.0036	0.0000	0.0000

Table S4. Vibrational modes and relative intensities from DFT calculations for Pt-DPTZ$_2$. The columns present: (1) mode number, (2) symmetry element, (3) frequency, and (4-7) four estimates of intensity, as discussed in the text. Each of the intensity columns are normalized to the most intense feature above 250 cm^{-1}. Peaks in HREEL spectra include intensity from both impact scattering and dipole scattering modes, which are best estimated by $\frac{1}{f_\alpha}\left|\frac{\delta P}{\delta Q_\alpha}\right|^2$ (column 5) and by $\frac{1}{f_\alpha^3}\left|\frac{\delta P_z}{\delta Q_\alpha}\right|^2$ (column 7), respectively.[9]

Mode, α	sym	frequency, f_α (cm^{-1})	$\left\|\frac{\delta P}{\delta Q_\alpha}\right\|^2$	$\frac{1}{f_\alpha}\left\|\frac{\delta P}{\delta Q_\alpha}\right\|^2$	$\left\|\frac{\delta P_z}{\delta Q_\alpha}\right\|^2$	$\frac{1}{f_\alpha^3}\left\|\frac{\delta P_z}{\delta Q_\alpha}\right\|^2$
1	AU	14	0.0006	0.0116	0.0016	219.0096
2	AU	29	0.0212	0.0051	0.0015	22.4639
3	BG	37	0.0000	0.0000	0.0000	0.0000
4	BG	39	0.0150	0.0000	0.0000	0.0000
5	AU	43	0.0000	0.0644	0.0278	130.2926
6	BU	45	0.0012	0.0121	0.0000	0.0000
7	AU	53	0.0000	0.1536	0.0823	202.0744
8	AG	67	0.0000	0.0000	0.0000	0.0000
9	BG	104	0.0004	0.0000	0.0000	0.0000
10	AU	109	0.0000	0.0043	0.0048	1.3611
11	BG	116	0.0037	0.0000	0.0000	0.0000
12	AU	131	0.0016	0.0059	0.0078	1.2721
13	BU	134	0.0000	0.0125	0.0000	0.0000
14	BG	149	0.0141	0.0000	0.0000	0.0000
15	AG	169	0.0450	0.0000	0.0000	0.0000
16	BU	181	0.0000	0.0202	0.0000	0.0000
17	AG	187	0.0000	0.0000	0.0000	0.0000
18	AU	198	0.1981	0.0014	0.0029	0.1360
19	BG	200	0.0000	0.0000	0.0000	0.0000
20	AU	211	0.0254	0.0034	0.0073	0.2871
21	BU	225	0.0000	0.0021	0.0000	0.0000
22	AG	258	0.0000	0.0000	0.0000	0.0000
23	AG	269	0.0667	0.0000	0.0000	0.0000
24	BU	288	0.0000	0.0091	0.0000	0.0000
25	BG	327	0.0988	0.0000	0.0000	0.0000
26	BU	329	0.0000	0.0140	0.0000	0.0000
27	AU	331	0.0895	0.0005	0.0016	0.0158
28	AU	351	0.0000	0.0084	0.0296	0.2515
29	BG	356	0.0000	0.0000	0.0000	0.0000
30	AU	410	0.0054	0.0126	0.0521	0.2783
31	BG	410	0.0000	0.0000	0.0000	0.0000
32	AG	420	0.0019	0.0000	0.0000	0.0000
33	BU	425	0.0000	0.0245	0.0000	0.0000

34	AU	438	0.0000	0.0013	0.0056	0.0245
35	BG	439	0.0437	0.0000	0.0000	0.0000
36	BG	460	0.0006	0.0000	0.0000	0.0000
37	AG	462	0.0000	0.0000	0.0000	0.0000
38	BU	463	0.0836	0.0087	0.0000	0.0000
39	AU	470	0.0000	0.0052	0.0244	0.0865
40	BG	533	0.0169	0.0000	0.0000	0.0000
41	AG	535	0.0577	0.0000	0.0000	0.0000
42	AU	538	0.0000	0.0004	0.0024	0.0057
43	BU	556	0.0186	0.0353	0.0000	0.0000
44	AU	621	0.0000	0.1040	0.6514	1.0000
45	AG	622	0.3190	0.0000	0.0000	0.0000
46	BU	622	0.0035	0.0417	0.0000	0.0000
47	BG	630	0.0000	0.0000	0.0000	0.0000
48	AG	652	0.0137	0.0000	0.0000	0.0000
49	BU	657	0.0000	0.0011	0.0000	0.0000
50	AG	673	0.2078	0.0000	0.0000	0.0000
51	BU	678	0.0000	0.0799	0.0000	0.0000
52	BU	684	0.0000	0.0017	0.0000	0.0000
53	AG	688	0.0199	0.0000	0.0000	0.0000
54	BG	726	1.0000	0.0000	0.0000	0.0000
55	AU	728	0.0000	0.0085	0.0627	0.0597
56	AG	741	0.0502	0.0000	0.0000	0.0000
57	BU	741	0.0000	0.0757	0.0000	0.0000
58	AU	749	0.0000	0.0234	0.1772	0.1548
59	BG	751	0.0102	0.0000	0.0000	0.0000
60	AU	752	0.0000	0.0221	0.1679	0.1448
61	BG	755	0.1224	0.0000	0.0000	0.0000
62	AU	789	0.0000	0.1255	1.0000	0.7469
63	BG	789	0.0000	0.0000	0.0000	0.0000
64	AU	814	0.0734	0.0163	0.1340	0.0912
65	BG	814	0.1806	0.0000	0.0000	0.0000
66	BU	849	0.0000	0.2111	0.0000	0.0000
67	AG	852	0.0730	0.0000	0.0000	0.0000
68	AU	903	0.0000	0.0007	0.0064	0.0032
69	BG	904	0.1773	0.0000	0.0000	0.0000
70	AU	916	0.0000	0.0029	0.0273	0.0130
71	BG	916	0.0000	0.0000	0.0000	0.0000
72	AU	966	0.0083	0.0007	0.0069	0.0028
73	BG	966	0.0000	0.0000	0.0000	0.0000
74	AG	977	0.0000	0.0000	0.0000	0.0000
75	BU	969	0.3050	0.4769	0.0000	0.0000

76	BG	974	0.0000	0.0000	0.0000	0.0000
77	AU	974	0.0011	0.0016	0.0164	0.0062
78	AG	980	0.0000	0.0000	0.0000	0.0000
79	BU	981	0.0373	0.0576	0.0000	0.0000
80	AU	987	0.0003	0.0004	0.0045	0.0016
81	BG	987	0.0000	0.0000	0.0000	0.0000
82	BU	1014	0.1000	0.1495	0.0000	0.0000
83	AG	1014	0.0000	0.0000	0.0000	0.0000
84	AU	1024	0.0016	0.0023	0.0243	0.0079
85	BG	1024	0.0000	0.0000	0.0000	0.0000
86	AG	1034	0.0000	0.0000	0.0000	0.0000
87	BU	1037	0.0337	0.0492	0.0000	0.0000
88	AG	1038	0.0000	0.0000	0.0000	0.0000
89	BU	1039	0.0139	0.0203	0.0000	0.0000
90	BU	1062	0.2628	0.3749	0.0000	0.0000
91	AG	1065	0.0000	0.0000	0.0000	0.0000
92	AG	1070	0.0000	0.0000	0.0000	0.0000
93	BU	1074	0.0532	0.0750	0.0000	0.0000
94	AG	1093	0.0000	0.0000	0.0000	0.0000
95	BU	1094	0.0581	0.0804	0.0000	0.0000
96	AG	1100	0.0000	0.0000	0.0000	0.0000
97	AG	1114	0.0000	0.0000	0.0000	0.0000
98	BU	1114	0.1116	0.1518	0.0000	0.0000
99	BU	1118	0.2171	0.2942	0.0000	0.0000
100	AG	1143	0.0000	0.0000	0.0000	0.0000
101	BU	1143	0.0129	0.0171	0.0000	0.0000
102	AG	1154	0.0000	0.0000	0.0000	0.0000
103	BU	1155	0.0322	0.0423	0.0000	0.0000
104	AG	1158	0.0000	0.0000	0.0000	0.0000
105	BU	1165	0.0339	0.0440	0.0000	0.0000
106	AG	1249	0.0000	0.0000	0.0000	0.0000
107	BU	1253	0.0650	0.0785	0.0000	0.0000
108	BU	1267	0.2984	0.3568	0.0000	0.0000
109	AG	1277	0.0000	0.0000	0.0000	0.0000
110	BU	1281	0.0624	0.0738	0.0000	0.0000
111	AG	1282	0.0000	0.0000	0.0000	0.0000
112	AG	1291	0.0000	0.0000	0.0000	0.0000
113	BU	1293	0.0175	0.0206	0.0000	0.0000
114	BU	1316	0.0715	0.0823	0.0000	0.0000
115	AG	1318	0.0000	0.0000	0.0000	0.0000
116	BU	1324	0.1808	0.2070	0.0000	0.0000
117	AG	1330	0.0000	0.0000	0.0000	0.0000
118	BU	1411	0.3750	0.4026	0.0000	0.0000

119	AG	1415	0.0000	0.0000	0.0000	0.0000
120	AG	1438	0.0000	0.0000	0.0000	0.0000
121	BU	1439	0.0221	0.0233	0.0000	0.0000
122	AG	1445	0.0000	0.0000	0.0000	0.0000
123	BU	1446	0.0813	0.0852	0.0000	0.0000
124	BU	1469	0.1726	0.1781	0.0000	0.0000
125	AG	1471	0.0000	0.0000	0.0000	0.0000
126	BU	1474	0.2383	0.2449	0.0000	0.0000
127	AG	1488	0.0000	0.0000	0.0000	0.0000
128	BU	1515	1.0000	1.0000	0.0000	0.0000
129	AG	1522	0.0000	0.0000	0.0000	0.0000
130	BU	1543	0.0528	0.0518	0.0000	0.0000
131	AG	1548	0.0000	0.0000	0.0000	0.0000
132	BU	1578	0.0139	0.0134	0.0000	0.0000
133	AG	1578	0.0000	0.0000	0.0000	0.0000
134	BU	1587	0.1304	0.1244	0.0000	0.0000
135	AG	1588	0.0000	0.0000	0.0000	0.0000
136	AG	1603	0.0000	0.0000	0.0000	0.0000
137	BU	1604	0.0465	0.0440	0.0000	0.0000
138	BU	3066	0.0345	0.0171	0.0000	0.0000
139	AG	3066	0.0000	0.0000	0.0000	0.0000
140	BU	3095	0.0208	0.0102	0.0000	0.0000
141	AG	3095	0.0000	0.0000	0.0000	0.0000
142	BU	3103	0.0293	0.0143	0.0000	0.0000
143	AG	3103	0.0000	0.0000	0.0000	0.0000
144	BU	3108	0.0014	0.0007	0.0000	0.0000
145	AG	3108	0.0000	0.0000	0.0000	0.0000
146	BU	3113	0.0568	0.0276	0.0000	0.0000
147	AG	3113	0.0000	0.0000	0.0000	0.0000
148	BU	3126	0.0103	0.0050	0.0000	0.0000
149	AG	3126	0.0000	0.0000	0.0000	0.0000
150	BU	3138	0.0032	0.0015	0.0000	0.0000
151	AG	3138	0.0000	0.0000	0.0000	0.0000
152	BU	3146	0.0014	0.0007	0.0000	0.0000
153	AG	3146	0.0000	0.0000	0.0000	0.0000

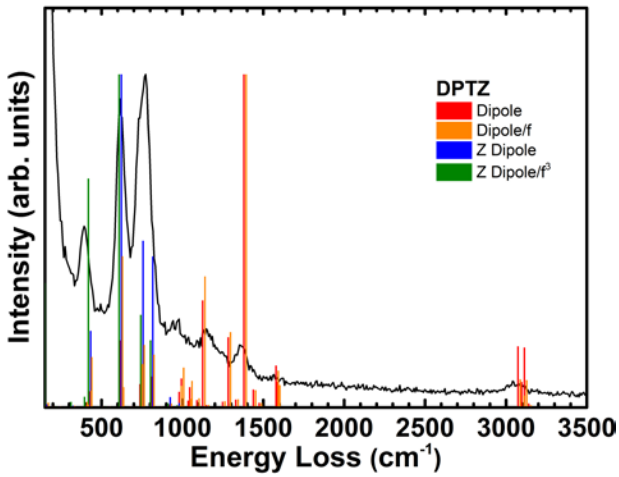

Figure S6. HREEL spectra of DPTZ on Ag(111) with bar graphs in four colors for comparison to the four intensity estimates presented in Table S3. "Dipole/f" (orange) best estimates impact scattering mode intensities. Assuming a flat lying molecule, "Z Dipole/f^3" (green) best estimates dipole scattering mode intensities.

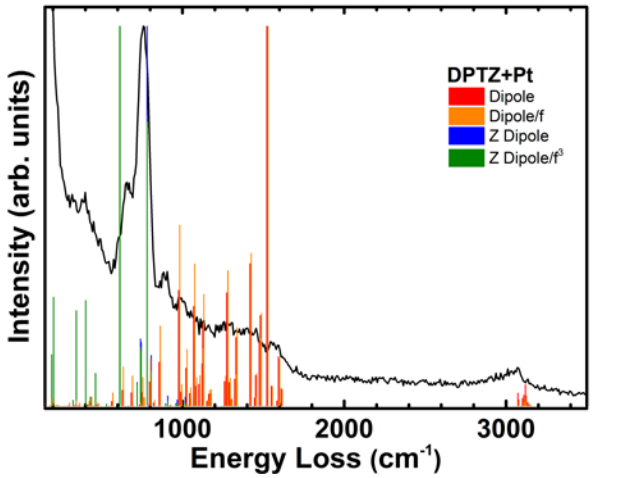

Figure S7. HREEL spectra of DPTZ+Pt on Ag(111) with bar graphs in four colors for comparison to the four intensity estimates presented in Table S3. "Dipole/f" (orange) best estimates impact scattering mode intensities. Assuming a flat lying molecule, "Z Dipole/f^3" (green) best estimates dipole scattering mode intensities.

References

1. Skomski, D.; Tempas, C. D.; Smith, K. A.; Tait, S. L., Redox-Active on-Surface Assembly of Metal–Organic Chains with Single-Site Pt(II). *J. Am. Chem. Soc.* **2014**, *136*, 9862-9865.
2. Wu, D.-Y.; Ren, B.; Jiang, Y.-X.; Xu, X.; Tian, Z.-Q., Density Functional Study and Normal-Mode Analysis of the Bindings and Vibrational Frequency Shifts of the Pyridine−M (M = Cu, Ag, Au, Cu^+, Ag^+, Au^+, and Pt) Complexes. *J. Phys. Chem. A* **2002**, *106*, 9042-9052.
3. Bard, A. J.; Parsons, R.; Jordan, J., *Standard Potentials in Aqueous Solution*; CRC Press, 1985; Vol. 6.
4. Bratsch, S. G., Standard Electrode Potentials and Temperature Coefficients in Water at 298.15 K. *J. Phys. Chem. Ref. Data* **1989**, *18*, 1-21.
5. Frisch, M. J.; Trucks, G. W.; Schlegel, H. B.; Scuseria, G. E.; Robb, M. A.; Cheeseman, J. R.; Scalmani, G.; Barone, V.; Mennucci, B.; Petersson, G. A., *et al.*, Gaussian 09, Revision B.01. Wallingford CT, 2009.
6. Giese, B.; Deacon, G. B.; Kuduk-Jaworska, J.; McNaughton, D., Density Functional Theory and Surface Enhanced Raman Spectroscopy Characterization of Novel Platinum Drugs. *Biopolymers* **2002**, *67*, 294-297.
7. Michalska, D.; Wysokiński, R., The Prediction of Raman Spectra of Platinum (II) Anticancer Drugs by Density Functional Theory. *Chem. Phys. Lett.* **2005**, *403*, 211-217.
8. Laury, M. L.; Carlson, M. J.; Wilson, A. K., Vibrational Frequency Scale Factors for Density Functional Theory and the Polarization Consistent Basis Sets. *J. Comput. Chem.* **2012**, *33*, 2380-2387.
9. Ibach, H.; Mills, D. L., *Electron Energy Loss Spectroscopy and Surface Vibrations*; Academic Press: London, 1982, p 5.